Radiology

ORIGINAL RESEARCH • VASCULAR AND INTERVENTIONAL RADIOLOGY

A Dual-layer Detector for Simultaneous Fluoroscopic and Nuclear Imaging

*Sandra van der Velden, MSc** • *Britt Kunnen, MSc** • *Wilco J. C. Koppert, PhD* • *Johannes H. L. Steenbergen, MSc* • *Martijn M. A. Dietze, MSc* • *Casper Beijst, PhD* • *Max A. Viergever, PhD* • *Marnix G. E. H. Lam, MD, PhD* • *Hugo W. A. M. de Jong, PhD*

From the Department of Radiology and Nuclear Medicine (S.V.D.V., B.K., W.J.C.K., J.H.L.S., M.M.A.D., C.B., M.G.E.H.L., H.W.A.M.D.J.) and Image Sciences Institute (S.V.D.V., B.K., M.M.A.D., M.A.V.), University Medical Center Utrecht, Utrecht University, PO Box 85500, 3508 GA Utrecht, the Netherlands. Received April 30, 2018; revision requested June 19; revision received October 31; accepted November 19. **Address correspondence to** S.V.D.V. (e-mail: *velden.sandra@gmail.com*).

Study supported by STW-VIDI research program (project number 12977), partially financed by the Netherlands Organization for Scientific Research; and the European Research Council European Union Horizon 2020 research and innovation program (grant no. 646734).

* S.V.D.V. and B.K. contributed equally to this work.

Conflicts of interest are listed at the end of this article.

Radiology 2019; 290:833–838 • https://doi.org/10.1148/radiol.2018180796 • Content codes: NM IR

Purpose: To develop and evaluate a dual-layer detector capable of acquiring intrinsically registered real-time fluoroscopic and nuclear images in the interventional radiology suite.

Materials and Methods: The dual-layer detector consists of an x-ray flat panel detector placed in front of a γ camera with cone beam collimator focused at the x-ray focal spot. This design relies on the x-ray detector absorbing the majority of the x-rays while it is more transparent to the higher energy γ photons. A prototype was built and dynamic phantom images were acquired. In addition, spatial resolution and system sensitivity (evaluated as counts detected within the energy window per second per megabecquerel) were measured with the prototype. Monte Carlo simulations for an improved system with varying flat panel compositions were performed to assess potential spatial resolution and system sensitivity.

Results: Experiments with the dual-layer detector prototype showed that spatial resolution of the nuclear images was unaffected by the addition of the flat panel (full width at half maximum, 13.6 mm at 15 cm from the collimator surface). However, addition of the flat panel lowered system sensitivity by 45%–60% because of the nonoptimized transmission of the flat panel. Simulations showed that an attenuation of 27%–35% of the γ rays in the flat panel could be achieved by decreasing the crystal thickness and housing attenuation of the flat panel.

Conclusion: A dual-layer detector was capable of acquiring real-time intrinsically registered hybrid images, which could aid interventional procedures involving radionuclides.

Online supplemental material is available for this article.

Hybrid imaging modalities are important to oncologic imaging because they combine anatomic and nuclear information. However, the use of hybrid imaging modalities (eg, SPECT/CT) in the interventional radiology suite is limited because of their bulky design (1). Interventional nuclear imaging is performed with γ probes or hand-held γ cameras, providing real-time feedback about the activity distribution. Interpretation of this information can be difficult because of the lack of coregistered anatomic information. Therefore, we aim to develop a real-time, simultaneous fluoroscopic and nuclear imaging device consisting of a c-arm with nuclear imaging capabilities.

In the design of Beijst et al (2) and van der Velden et al (3), four γ cameras with pinhole collimators were positioned at the side of the x-ray tube. Although the prototype showed that interventional hybrid imaging was feasible, this design required an intermediate reconstruction step and additional weight added to the already heavy x-ray tube. Also, it had a lower spatial resolution of the nuclear image close to the x-ray detector. Instead, we propose a dual-layer detector that does not require an intermediate reconstruction step, has better nuclear image resolution, and has better weight balance between x-ray source and detector.

The purpose of this study was to develop a dual-layer detector capable of acquiring intrinsically registered real-time fluoroscopic and nuclear images in the interventional radiology suite.

Materials and Methods

Philips Healthcare supported this research by providing an adapted x-ray flat panel detector. The authors had full control over the data and the information submitted for publication.

Geometry

The dual-layer detector consists of a γ camera with cone beam collimator placed behind a dynamic x-ray flat panel (Fig 1). The cone beam collimator is focused on the focal spot of the x-ray tube, resulting in intrinsically registered x-ray and nuclear images (Fig 1). The x-ray flat panel absorbs the majority of x-rays (30–120 keV) but is more

Summary

A dual-layer detector is capable of acquiring intrinsically registered real-time hybrid fluoroscopic and nuclear images in the intervention suite.

Implications for Patient Care

- Real-time hybrid fluoroscopic and nuclear imaging may provide physicians with valuable information regarding radionuclide distribution during interventional procedures involving radionuclides such as radioembolization.
- Availability of hybrid images in the interventional radiology suite could improve therapeutic efficiency of radioembolization procedures by allowing 1-day procedures.

transparent to higher energy (140 keV) γ rays, allowing simultaneous detection.

Authors (W.J.C.K. and J.H.L.S., both with 8 years of experience) built an experimental prototype of the dual-layer detector (Fig 2). The γ imaging part of the prototype consisted of a Diacam γ camera (Siemens Healthcare, Erlangen, Germany) mounted with a low-energy cone beam collimator (septal thickness, 0.25 mm; hole diameter, 1.90 mm; hole length, 40 mm; focal distance, 98 cm; Nuclear Fields, Vortum-Mullem, the Netherlands) (4). The γ camera had a 9.5-mm thallium-doped sodium iodide scintillation crystal and a field of view of 53.3 × 38.7 cm. The intrinsic resolution of the γ camera was 10-mm full width at half maximum as measured with a collimated point source without collimator.

The fluoroscopy part consisted of an x-ray tube of a Veradius c-arm (Philips Healthcare, Best, the Netherlands) and a commercially available Pixium 3040 flat panel (Trixell, Moirans, France) (5). The x-ray flat panel had a 750-μm thallium-doped cesium iodide detection layer, 154-μm pixel pitch, a field of view of 29.6 × 38.2 cm, and a total thickness of 7.5 cm. The flat panel was first modified by Philips Healthcare to improve the transmission of γ rays over the original detector by removing the lead shielding and some excess aluminum at the backside of the assembly.

Phantom Experiments

To illustrate potential applications of the dual-layer detector, two phantom experiments were performed (S.V.D.V. and B.K., with 4 years and 3 years of experience, respectively) in which dynamic nuclear and fluoroscopic images were simultaneously acquired. In the first experiment, an 8.4-MBq cobalt 57 pen marker was moved within the thorax of the RS-800 phantom (Radiological Support Devices, Long Beach, Calif). The thorax was filled with air and the heart, liver, and lungs were removed while all bone structures of the thorax were present.

In the second experiment, a liver-shaped phantom containing a 40-mm diameter sphere that represented a liver tumor was positioned on a translating stage to simulate breathing motion (amplitude, 2 cm; 5-second period). The sphere was filled with 16 MBq of technetium 99m (^{99m}Tc) and the background compartment was filled with 83 MBq of ^{99m}Tc (concentration ratio, 1:10), which represented a ^{99m}Tc macroaggregated albumin procedure preceding yttrium 90 radioembolization (6).

For both phantom experiments, hybrid images were acquired at 4 Hz. Figure 3 shows the data acquisition scheme (Appendix E1 [online]).

Nuclear Image Quality

To assess nuclear image quality, static measurements were performed (S.V.D.V. and B.K.) by using a 4-MBq ^{99m}Tc point source positioned at varying distances (range, 11.5–37.5 cm) from the collimator surface with 60-second acquisition time with and without flat panel in place to study the influence of the flat panel on nuclear image spatial resolution and system sensitivity. Counts were acquired in a 15% energy window centered at 140 keV. Pixel size was 2 × 2 mm. Spatial resolution was defined as the full width at half maximum of the point spread function. System sensitivity was expressed in counts per second per megabecquerel detected within the energy window. In addition, system sensitivity was measured by using a 200-MBq ^{99m}Tc flood source of 53 × 40 cm.

Simulations

The prototype system was Monte Carlo simulated by using the Monte Carlo n-Particle Transport Code 1.0 (Los Alamos National Laboratory, Los Alamos, NM; S.V.D.V. and B.K.) (11). Because the exact composition of the flat panel was confidential and therefore not disclosed by the manufacturer, the flat panel was modeled as 750-μm cesium iodide, 700-μm silicon (read-out layer), and 26-mm aluminum to match the system sensitivity of the prototype system. The total thickness of the modeled flat panel was identical to that of the prototype flat panel (7.5 cm, with the remaining 47.5 mm modeled as air).

On the basis of this model, improved systems were simulated by reducing the amount of aluminum to 7 mm, reducing the flat panel thickness to 1 cm (thin flat panel), varying the cesium iodide thickness (range, 0.3–0.75 mm), and simulating an intrinsic spatial resolution of the γ camera of 3-mm full width at half maximum. Simulation details can be found in Appendix E1 (online).

Results

Phantom Experiments

Figures 4 and 5 show single-frame images of the real-time, simultaneously acquired hybrid video of both phantoms (Movies E1, E2 [online]), with the fluoroscopic image in gray scale and the nuclear image in color overlay. Visual inspection of the images showed that good spatial overlap was obtained and no artifacts were visible in either the fluoroscopic or nuclear images (agreement by all authors, including M.G.E.H.L., with > 20 years of experience). This shows that the presence of the radioactive tracer had no influence on the quality of the fluoroscopic image. In addition, nuclear images could be acquired with short frame durations, despite the attenuation and scatter of γ rays by the flat panel.

Nuclear Image Quality

Figure 6a, 6b shows the measured system sensitivity and spatial resolution of the prototype, with and without flat panel,

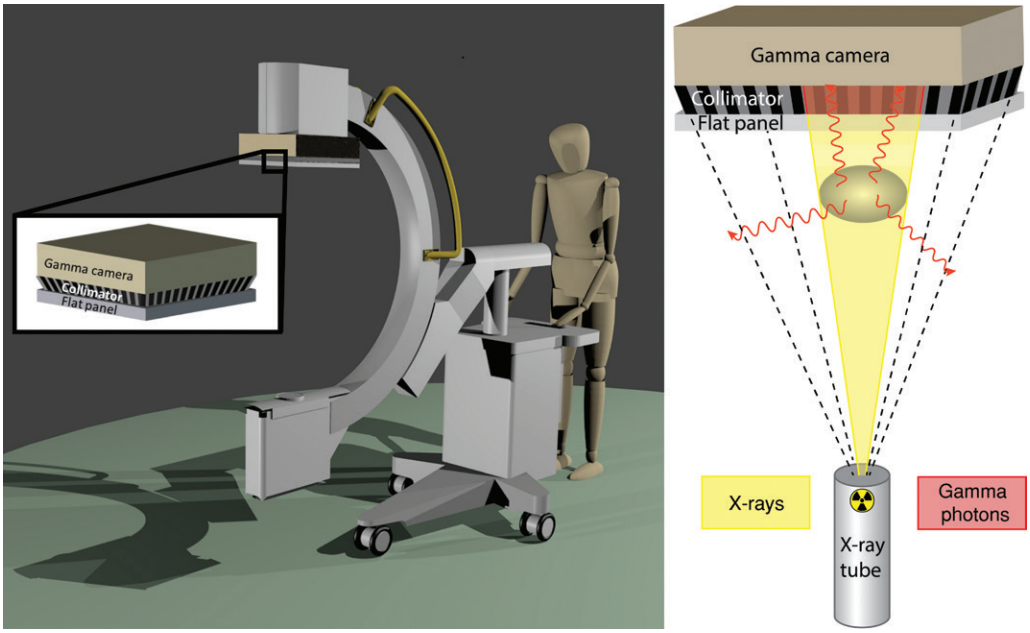

Figure 1: Rendering of a mobile c-arm with the proposed dual-layer detector, consisting of a γ camera, cone beam collimator and x-ray flat panel (left); and schematic overview of the principle of simultaneous detection of nuclear and radiographic images (right).

and the simulations of the prototype system with flat panel. The simulations were in agreement with the measurements of the prototype (difference in system sensitivity and spatial resolution, <14% and <9%, respectively). For the point source, measured at the center of the camera, incorporating the flat panel into the setup reduced the system sensitivity by 60%. Reduction was 45% when measured with the flood source. The difference in measured system sensitivity represents the inhomogeneity of the flat panel. Spatial resolution was unaffected by addition of the flat panel (difference < 7%).

Figure 6c, 6d shows the simulated system sensitivity and spatial resolution of the improved systems. Incorporating a thin flat panel into the setup reduced the system sensitivity by 27%–35%, depending on the cesium iodide crystal thickness. Improving the intrinsic resolution of the γ camera did not influence the system sensitivity. Spatial resolution was unaffected (difference of < 2%) by reducing the flat panel thickness or varying cesium iodide thickness. However, a thinner flat panel allowed smaller source-collimator distances, which improved the spatial resolution. Improving the intrinsic resolution of the γ camera also improved the spatial resolution of the system.

Discussion

Interventional procedures could benefit from real-time intrinsically registered hybrid images for improved localization and treatment guidance. Simulations and measurements with the prototype system demonstrated that a dual-layer detector, consisting of a γ camera with cone beam collimator and x-ray flat panel, was capable of acquiring such hybrid images. Addition of the flat panel did not affect spatial resolution of the nuclear image, and system sensitivity decreased by 45%–60%.

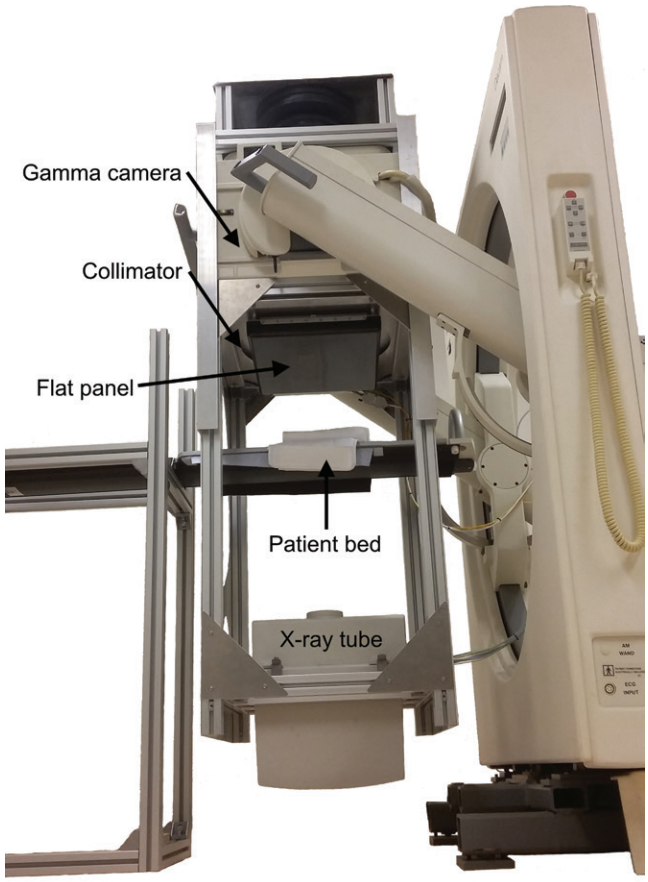

Figure 2: Prototype setup consisting of a γ camera with cone beam collimator (focus at 98 cm), modified flat panel, and x-ray tube.

Availability of hybrid images would potentially benefit multiple procedures such as sentinel node procedures, biopsies, and radioembolization procedures. For radioembolization procedures,

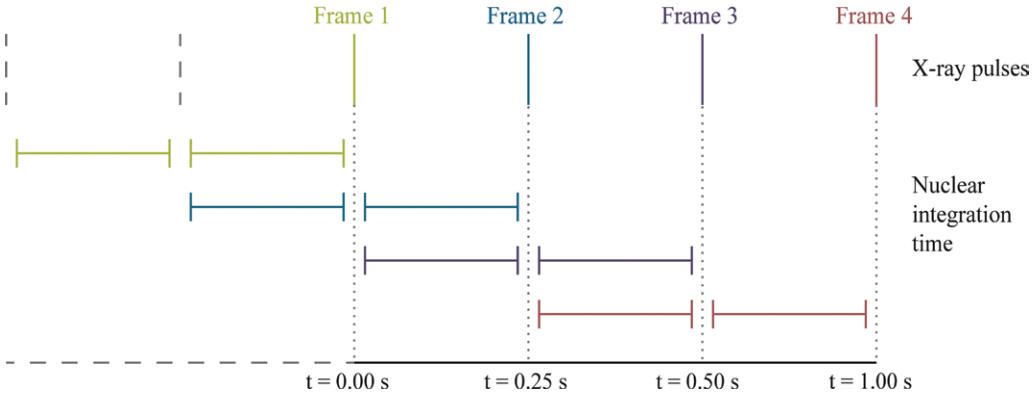

Figure 3: Schematic overview of hybrid data acquisition scheme. Every 250 msec, list-mode data of the prior 500 msec were binned into image frames, which were visualized at a frame rate of 4 Hz. List-mode data acquired during and shortly after the x-ray pulses were left out (21 msec per x-ray pulse).

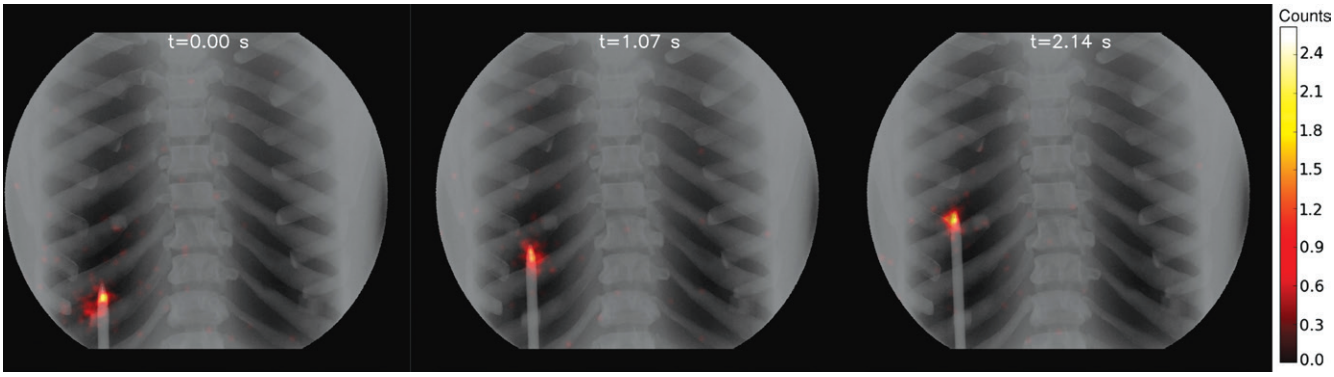

Figure 4: Single-frame images (Δ*t* = 1.07 seconds) of the video of a cobalt 57 pen marker moving inside the thorax of the RS-800 phantom (Movie E1 [online]). Fluoroscopic images are shown in gray scale and nuclear images are shown in color overlay scaled between 0 and the maximum number of counts.

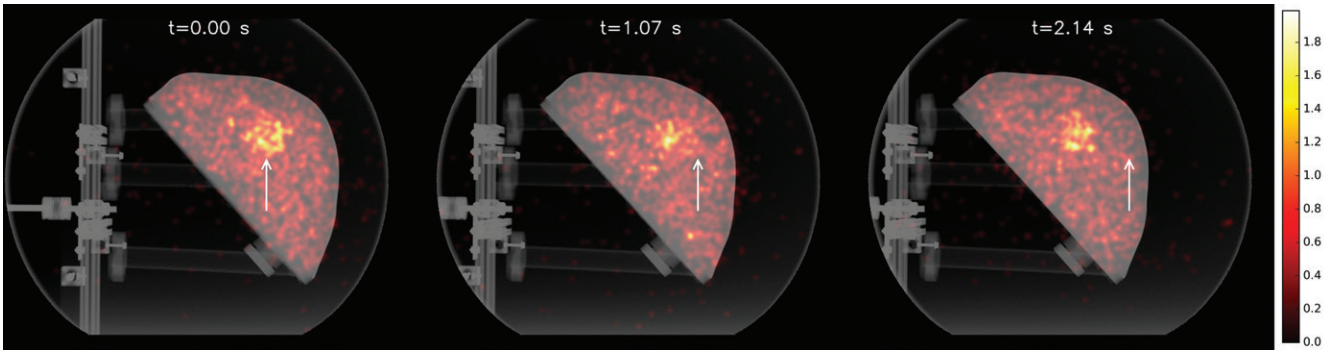

Figure 5: Single-frame images (Δ*t* = 1.07 seconds) of the video of the moving liver-shaped phantom acquired with the prototype setup (Movie E2 [online]). Fluoroscopic images are shown in gray scale and nuclear images are shown in color overlay scaled between 0 and the maximum number of counts. Arrows indicates the position of the hot sphere as it appeared in the left-side frame (*t* = 0.00 seconds).

the main advantage is that patients will not have to be transferred to the nuclear medicine department for assessment of the pretreatment procedure with ^{99m}Tc-macroaggregated albumin. This would make the procedure more time efficient and would allow for 1-day radioembolization procedures (7,8). In a 1-day procedure, the vascular sheath is not removed, ensuring equal injection position for ^{99m}Tc-macroaggregated albumin and microspheres. When nuclear images can be acquired in the intervention room, movement of the vascular sheath is limited because the patient does not have to change beds for assessment of the ^{99m}Tc-macroaggregated albumin distribution. This improves the prognostic power of the pretreatment procedure (9). However, in principle, any procedure that uses radionuclides and fluoroscopic imaging could benefit from our dual-layer detector.

Transmission of γ rays through the flat panel can be substantially improved by reducing the amount of aluminum surrounding the flat panel. In addition, repositioning the read-out electronics would improve homogeneity of the γ ray transmission.

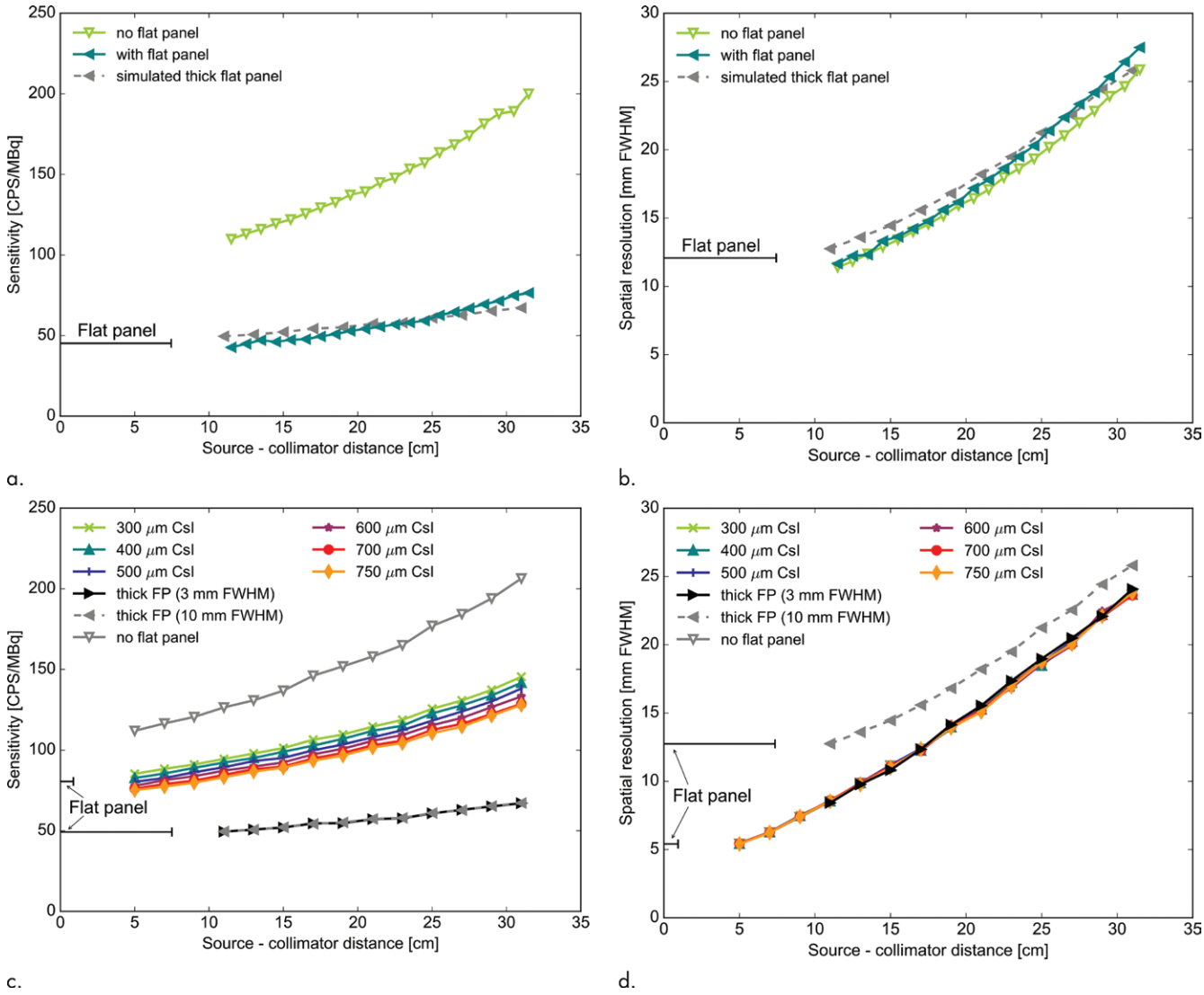

Figure 6: Graphs show measured and simulated **(a)** system sensitivity and **(b)** spatial resolution of the prototype system. The simulated thick flat panel was modeled to match these measurements. **(c)** Simulated system sensitivity and **(d)** simulated spatial resolution for the current thick flat panel and the modeled thin flat panels. The thickness of the flat panel is indicated by the horizontal line. CPS = counts per second, CsI = cesium iodide, FP = flat panel, FWHM = full width at half maximum.

The position of some large electronic components explains the difference in system sensitivity when measured with a point source compared with a flood source (60% and 45% reduced system sensitivity, respectively).

Modifications to our prototype flat panel only affected the housing and therefore did not influence its imaging properties, so from the fluoroscopic point of view every fluoroscopic setting can be used. However, from a nuclear point of view, the current prototype allows the use of 40–80-kVp tube voltages, depending on the tube current. For our phantom experiments, fluoroscopic images were acquired at approximately 50 kVp because the phantoms were small and did not require high tube voltages. In clinical practice, higher tube voltages are used. Although higher tube voltages cause more photons to penetrate the x-ray detector and create interactions in the γ camera, we believe that this effect can be mitigated by modification of the photomultiplier tube circuitry, and/or the addition of a high pass filter, and/or by performing interleaved measurements (required when tube voltage approaches photopeak energy) (10). Such interleaved measurements were used for the acquisition of the phantom images and assumed in our simulations, obviating simulation of the x-ray pulses.

A limitation of our proposed detector is the reduced system sensitivity of the γ camera because of the attenuation in the flat panel and the short frame duration required for real-time imaging. Although these factors will negatively influence nuclear image quality in terms of contrast and noise, the aim of our system is not to provide the physician with images of the highest diagnostic quality. In interventional procedures, the diminished nuclear image quality may be compensated by providing additional information that is otherwise not available. Also, image quality may be improved by image processing, which exploits the dynamic nature of the image data by frame averaging and is commonly performed at fluoroscopy.

In conclusion, we have demonstrated the feasibility of acquiring real-time and intrinsically registered fluoroscopic and nuclear images of the same field of view by means of a dual-layer detector. Such hybrid images may be used advantageously in interventional procedures involving radionuclides such as radioembolization. In a more mature setup, we plan to redesign the aluminum housing of the flat panel and reposition the read-out electronics. This will result in the transmission of more γ photons through the flat panel. The final design of our setup will be a trade-off between nuclear and fluoroscopic image quality. Regarding flat panel composition, a thicker cesium iodide layer would lead to both better fluoroscopic dose efficiency and a lower sensitivity for γ photons. The required cesium iodide thickness will be further investigated in future research.

Author contributions: Guarantors of integrity of entire study, S.V.D.V., B.K., H.W.A.M.D.J.; study concepts/study design or data acquisition or data analysis/interpretation, all authors; manuscript drafting or manuscript revision for important intellectual content, all authors; approval of final version of submitted manuscript, all authors; agrees to ensure any questions related to the work are appropriately resolved, all authors; literature research, S.V.D.V., B.K., H.W.A.M.D.J.; experimental studies, S.V.D.V., B.K., W.J.C.K., J.H.L.S., C.B., H.W.A.M.D.J.; statistical analysis, S.V.D.V., B.K., W.J.C.K., H.W.A.M.D.J.; and manuscript editing, all authors

Disclosures of Conflicts of Interest: **S.V.D.V.** Activities related to the present article: disclosed no relevant relationships. Activities not related to the present article: disclosed money to author's institution from Quirem Medical/Terumo for royalties and research support. Other relationships: disclosed no relevant relationships. **B.K.** Activities related to the present article: disclosed no relevant relationships. Activities not related to the present article: disclosed money to author's institution from Quirem Medical/Terumo for royalties and research support. Other relationships: disclosed no relevant relationships. **W.J.C.K.** Activities related to the present article: disclosed that Philips loaned an x-ray flat panel detector and x-ray c-arm to author's institution for this study. Activities not related to the present article: disclosed no relevant relationships. Other relationships: disclosed no relevant relationships. **J.H.L.S.** Activities related to the present article: disclosed that Philips loaned an x-ray flat panel detector and x-ray c-arm to author's institution for this study. Activities not related to the present article: disclosed no relevant relationships. Other relationships: disclosed no relevant relationships. **M.M.A.D.** disclosed no relevant relationships. **C.B.** disclosed no relevant relationships. **M.A.V.** disclosed no relevant relationships. **M.G.E.H.L.** Activities related to the present article: disclosed that Philips loaned an x-ray flat panel detector and x-ray c-arm to author's institution for this study. Activities not related to the present article: disclosed money to author's institution from Terumo and BTG for consultancy; disclosed payment to author for lectures including service on speakers bureaus from BTG; disclosed money to author's institution for royalties from Quirem Medical/Terumo. Other relationships: disclosed no relevant relationships. **H.W.A.M.D.J.** disclosed no relevant relationships.

References

1. Shyn PB. Interventional positron emission tomography/computed tomography: state-of-the-art. Tech Vasc Interv Radiol 2013;16(3):182–190.
2. Beijst C, Elschot M, Viergever MA, de Jong HWAM. Toward simultaneous real-time fluoroscopic and nuclear imaging in the intervention room. Radiology 2016;278(1):232–238.
3. van der Velden S, Beijst C, Viergever MA, de Jong HWAM. Simultaneous fluoroscopic and nuclear imaging: impact of collimator choice on nuclear image quality. Med Phys 2017;44(1):249–261.
4. Jaszczak RJ, Greer KL, Coleman RE. SPECT using a specially designed cone beam collimator. J Nucl Med 1988;29(8):1398–1405.
5. Ducourant T, Wirth T, Bacher G, et al. Latest advancements in state-of-the-art aSi-based x-ray flat panel detectors. In: Chen GH, Lo JY, Gilat Schmidt T, eds. Proceedings of SPIE: medical imaging 2018—physics of medical imaging. Vol 10573. Bellingham, Wash: International Society for Optics and Photonics, 2018; 105735V.
6. Giammarile F, Bodei L, Chiesa C, et al. EANM procedure guideline for the treatment of liver cancer and liver metastases with intra-arterial radioactive compounds. Eur J Nucl Med Mol Imaging 2011;38(7):1393–1406.
7. Gabr A, Kallini JR, Gates VL, et al. Same-day ^{90}Y radioembolization: implementing a new treatment paradigm. Eur J Nucl Med Mol Imaging 2016;43(13):2353–2359.
8. Gates VL, Marshall KG, Salzig K, Williams M, Lewandowski RJ, Salem R. Outpatient single-session yttrium-90 glass microsphere radioembolization. J Vasc Interv Radiol 2014;25(2):266–270.
9. Garin E, Edeline J, Rolland Y. High impact of preferential flow on 99mTc-MAA and 90Y-loaded microsphere uptake correlation. J Nucl Med 2016;57(11):1829–1830.
10. Koppert WJC, van der Velden S, Steenbergen JHL, de Jong HWAM. Impact of intense x-ray pulses on a NaI(Tl)-based gamma camera. Phys Med Biol 2018;63(6):065006.
11. Goorley T, James M, Booth T, et al. Initial MCNP6 release overview. Nuclear Tech 2012;180(3):298–315.